Coating deformations in the continuous hot-dipped galvanizing process

Graeme Hocking
Murdoch University

Winston Sweatman
Massey University

Melanie Roberts
University of Western Australia

Alistair Fitt
University of Southampton

Abstract

The coating of steel by dipping through a molten alloy and then stripping off excess coating using an air jet is considered. A first-order partial differential equation is derived and solved both to obtain the steady-state coating shape and to determine the evolution of any defects that may form. Analysis of possible mechanisms for defect formation is discussed. A simple heat transfer model is developed to consider the possibility of phase changes over the relevant section of the process.

1 Introduction and problem description

During the production of steel strips, the steel surface is usually coated with a layer of metallic alloy (e.g. zinc/aluminium) to protect it from corrosion. A mechanism for achieving this is the "continuous hot-dipped galvanising process" for which the steel strip is passed through a bath of the molten metal coating. The steel surface is protected from corrosion prior to entry into the bath. After passing through and being coated by the molten metal the strip is pulled upward until eventually the metal coating cools and solidifies.

The thickness of the metal coating is controlled by a pair of air knives on either side of the ascending steel strip. Each of these air knives fires air at a high pressure along a horizontal line across the rising strip. The air forces some of the molten metal to return downwards into the bath. Above the air knives there is no further loss of metal material.

During recent developments in the production process, problems with the quality of the surface coating have arisen, in particular with some new advanced alloy coatings. Associated with each set of process conditions, such as the speed of the strip and the alloy used, there is an air knife pressure below which the coating is satisfactory but above which coating defects may appear. The defects take the form of waves, lines and pocks. Of these the pocks are the most serious as they are the deepest and correspond to a substantial thinning of the coating and a dramatic reduction of the corrosion protection. Each pock has dimensions of the order

of millimetres, is broader in the horizontal direction, has a downstream bump and has a depth of 70-90% of the usual alloy coating thickness.

The MISG group developed an equation to model the process, considering the evolution of the shape of the coating. They further investigated heat transfer and possible mechanisms for the formation of defects.

In order to obtain a steady-state solution and also to consider the time evolution of the surface coating, the process is modelled as a two-dimensional, uni-directional fluid flow. An equation is derived for the dynamics of the coating layer including all processes that are thought might be of importance. The magnitudes of the different terms including surface tension, shear, heat transfer, air pressure and gravity, were estimated from typical parameter values to determine their relative importance. Surface tension was found to have only a small effect, while the air pressure and shear appeared to be the dominant terms. Only in the absence of the air knife was gravity found to play a significant role.

The resulting "simplified" equation is a first-order partial differential equation, the solution of which turns out to be rather delicate depending on the upstream flux condition. This equation is consistent with earlier models described in the literature and the model used by industry, see [1, 4, 5, 7]. It is derived in Section 2, and then used to obtain a steady-state solution (Section 3) and to examine the stability and evolution of perturbations in both time and space (Sections 4 and 5).

This model is only valid, however, if the heat transfer is insufficient to cause solidification over the region of interest. This possibility is considered in Section 6.

Possible mechanisms for pock formation were discussed. Dissolved bubbles in the molten coating seemed unlikely, but the possibility of entrapment might be investigated by experiment. Contamination of the metal in the bath or in the air is already being investigated by the company. Vapour explosions were ruled out by the industry representatives. However, it seemed plausible that impacts of particles, entrained in the air knife, might produce a fracture in the oxide film. This is discussed in Section 7. The report finishes with some discussion and suggestions for future work.

2 Mathematical modelling of the coating process

To develop a mathematical model for the coating process, we adopt the coordinate scheme shown in Figure 1. The flow is assumed to be two-dimensional, incompressible, laminar and unsteady.

The flow is governed by the two-dimensional Navier-Stokes equations

$$u_t + uu_x + wu_z = -\frac{1}{\rho}p_x + \frac{\mu}{\rho}(u_{xx} + u_{zz}) - g \tag{1}$$

$$w_t + uw_x + ww_z = -\frac{1}{\rho}p_z + \frac{\mu}{\rho}(w_{xx} + w_{zz}) \tag{2}$$

$$u_x + w_z = 0 \tag{3}$$

where t denotes time, x and z respectively denote the vertical and horizontal coordinates, $\vec{q} = (u, w)$ denotes the fluid velocity, p denotes pressure, ρ denotes density, μ denotes dynamic viscosity, subscripts are used to indicate differentiation and g is the acceleration due to gravity.

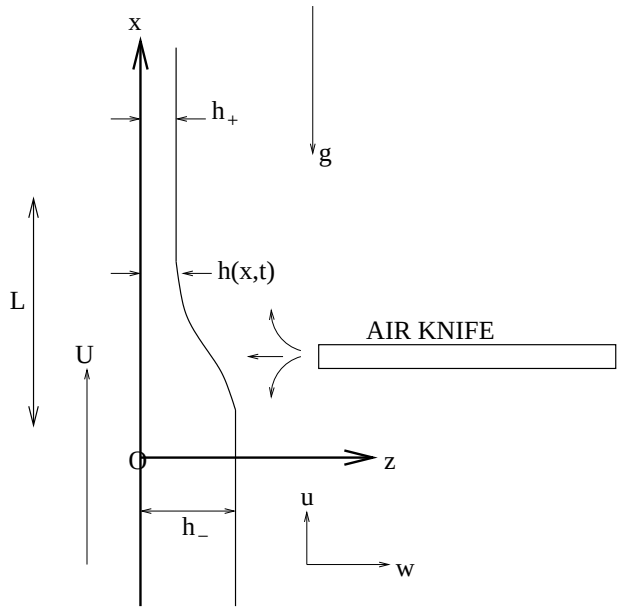

Figure 1: Schematic of coordinate system and nomenclature

In addition to the initial condition that is required to specify the problem, the boundary conditions are

$$u = U, \quad w = 0 \quad \text{at} \;\; z = 0 \tag{4}$$

$$\mu u_z = \tau_a(x), \quad p - p_a(x) = -\gamma\kappa, \quad h_t + uh_x = w \;\; \text{at} \;\; z = h(x,t). \tag{5}$$

Here U denotes the speed of the coating substrate, $z = h(x,t)$ is the equation of the free surface of the coating layer, γ denotes surface tension, κ denotes curvature, and $p_a(x)$ and $\tau_a(x)$ (both of which we assume to be specified) are respectively the pressure and the shear stress that are applied by the action of the air knife. As the rate of change of h with x is small, the curvature $\kappa \sim h_{xx}$.

The equations (1)-(3) and boundary conditions (4)-(5) may be non-dimensionalised. We set $x = L\bar{x}$, $z = \epsilon L\bar{z}$, $u = U\bar{u}$, $w = \epsilon U\bar{w}$, $t = (L/U)\bar{t}$, $p = (\mu U/\epsilon^2 L)\bar{p}$, $h = \epsilon L\bar{h}$, $\tau_a(x) = (\mu U/\epsilon L)G(x)$ and $p_a(x) = (\mu U/\epsilon^2 L)P(x)$. Here bars denote non-dimensional variables, h_0 denotes a typical value of h, L denotes a typical length over which the air knife is active, and $\epsilon = h_0/L << 1$. With these scalings, the equations and boundary conditions become, to leading order,

$$p_x = u_{zz} - S, \quad p_z = 0, \quad u_x + w_z = 0 \tag{6}$$

$$u = 1, \quad w = 0 \quad \text{at} \;\; z = 0 \tag{7}$$

$$u_z = G(x), \quad p - P(x) = -Ch_{xx}, \quad h_t + uh_x = w \quad \text{at} \;\; z = h, \tag{8}$$

where the overbars have been dropped for convenience,

$$S = \frac{\epsilon^2 \rho g L^2}{\mu U}, \quad C = \frac{\epsilon^3 \gamma}{\mu U}$$

(S is the Stokes number and C is ϵ^3 times the Capillary number Ca) and, according to the usual "thin layer" assumptions, terms multiplied by $\epsilon^2 Re = h_0^2 \mu U/L^3 \sim 5 \times 10^{-5}$ (see values

in Appendix 1) have been ignored. We may now solve (6)-(8). We find that

$$p = P(x) - Ch_{xx} \tag{9}$$

$$u = (S + P'(x) - Ch_{xxx})\left(\frac{1}{2}z^2 - hz\right) + zG(x) + 1 \tag{10}$$

$$w = -(P''(x) - Ch_{xxxx})\left(\frac{1}{6}z^3 - \frac{1}{2}hz^2\right) +$$

$$\frac{1}{2}z^2 h_x(S + P'(x) - Ch_{xxx}) - \frac{1}{2}z^2 G'(x). \tag{11}$$

The pressure and velocity components in (9)-(11) satisfy the equations (6) and all of the boundary conditions (7) and (8) except for the final one - using (9)-(11) in this final condition now gives a PDE that governs the evolution of $h(x,t)$ in the form

$$h_t + \left(h + \frac{1}{2}h^2 G(x) - \frac{1}{3}h^3(S + P'(x) - Ch_{xxx})\right)_x = 0. \tag{12}$$

We will shortly discuss the matter of initial and boundary conditions for this equation, and how a solution with small non-uniformities might evolve to form waves, lines or pocks. First, however, we consider the matter of steady-state solutions to (12).

3 Steady state solutions

Surface tension will be neglected by setting $C \sim 10^{-6}$ equal to zero. To examine steady-state solutions to (12), consider the flux

$$Q = f(h,x) = h + \frac{h^2}{2}G(x) - \frac{h^3}{3}(S + P'(x)). \tag{13}$$

In areas of the flow where the air knife is not present (or the effects of the blowing and the shear stress are negligibly small), we have

$$Q = f_0(h) = h - \frac{Sh^3}{3}.$$

In these regions h is therefore constant, and can take one of the two values h_-, h_+ where $0 < Q < 2/(3\sqrt{S})$ and $0 < h_+ < S^{-1/2} < h_- < \sqrt{3/S}$ (see Figure 2).

When the air knife operates, its desired effect is to produce a permanent diminution in the coating layer. We therefore need to identify a steady-state solution that somehow changes continuously from h_- to $h_+ < h_-$ as x increases.

As x varies, the flux Q is constant. However, the coefficients of the cubic expression, equation (13), vary continuously with changes in the shear stress and pressure ($G(x)$ and $P(x)$). For any value of x, the value of h is determined as a root of this cubic expression. The values of h neighbouring h_- and h_+ correspond to different roots. So for a continuous join the cubic must possess a double root at some point $x = x_c$, for which we will suppose $h = h_c$. Thus

$$\frac{\partial f}{\partial h}(h_c, x_c) = 1 + h_c G(x_c) - h_c^2[S + P'(x_c)] = 0. \tag{14}$$

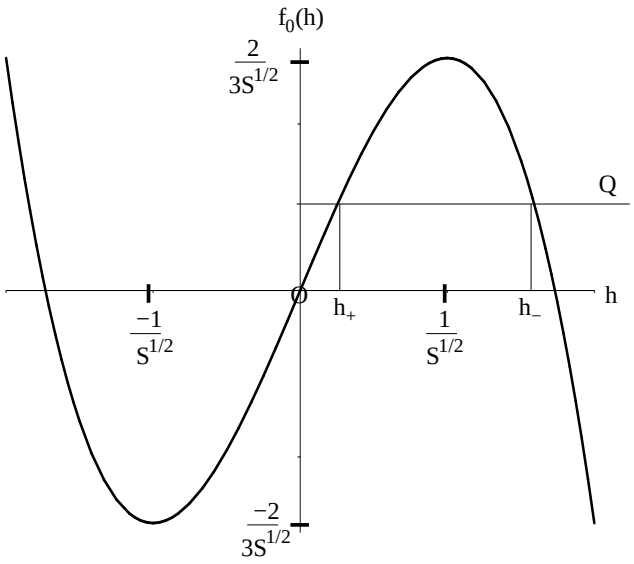

Figure 2: Cubic governing flux for case with no blowing

From (13), we now find that, since the flux Q must be identical for all values of x,

$$\frac{dQ}{dx} = 0 = h'[1 + hG(x) - h^2(S + P'(x))] + \frac{h^2}{2}G'(x) - \frac{h^3}{3}P''(x).$$

Evaluating this at $x = x_c$ and using (14) now shows that, since $h_c \neq 0$,

$$G'(x_c) = \frac{2}{3}h_c P''(x_c). \tag{15}$$

Possible locations of x_c and values of h_c are therefore determined by solutions to (14) and (15), whence the flux Q_c that is required to allow a smooth connection between h_- and h_+ is given by $Q_c = f(h_c, x_c)$. Note also that by differentiating (13), we find that

$$h'(x) = \frac{-\frac{h^2}{2}G'(x) + \frac{h^3}{3}P''(x)}{1 + hG(x) - h^2(S + P'(x))}. \tag{16}$$

At $x = x_c$ both the numerator and denominator of (16) are zero, so to find the slope h'_c of the steady state solution at x_c L'Hôpital's rule must be used. With rearrangement this gives a quadratic expression for h'_c.

It should be noted that one way of interpreting (14) and (15) is that they cause Q_c to be chosen by "minimising the maximum flux as a function of x". There appears, however, to be no real physical justification for this general principle - it is simply serendipity that this process corresponds to solving the "connection conditions" that allow a smooth joining of h_- to h_+.

Figure 3 shows a typical steady-state solution. In this case we have chosen the air knife blowing details as

$$S = \frac{1}{2}, \quad P(x) = 2e^{-x^2}, \quad G(x) = \frac{2x}{1 + x^4}. \tag{17}$$

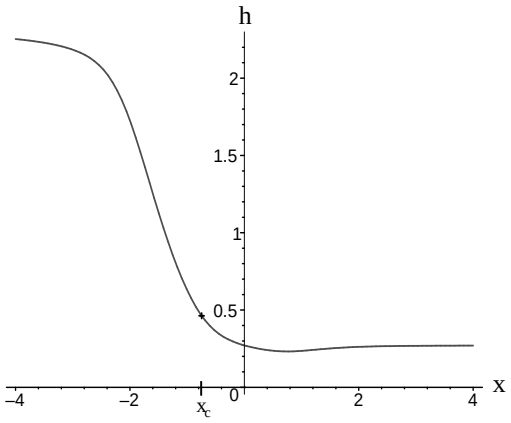

Figure 3: Typical steady-state solution (see text for parameter details)

These choices are not empirically determined functions but are chosen merely to illustrate the behaviour. They do have the correct qualitative behaviour near the critical stripping point. Using the methodology described above, it transpires that $x_c \sim -0.746$, $h_c \sim 0.463$, the flux is given by $Q_c \sim 0.268$, the upstream coating thickness by $h_- \sim 2.303$ and the downstream thickness by $h_+ \sim 0.271$.

4 The evolution of small disturbances

Suppose now that a coating process is established and running in steady state, with the coating varying smoothly as x increases from h_- to h_+ under the action of the air knife as described in Section 3. Thus $h = h_0(x)$ where h_0 is determined by

$$h_0 + \frac{h_0^2}{2}G(x) - \frac{h_0^3}{3}(S + P'(x)) = Q_c$$

and Q_c by solutions to (14) and (15). Let us now introduce a small disturbance into the governing equation (12) by setting $h(x,t) = h_0(x) + \delta h_1(x,t)$ where $\delta << 1$, and try to determine under what circumstances this disturbance might grow, decay or propagate. At $O(\delta)$, we find (neglecting the surface tension term) that $h_1(x,t)$ satisfies the equation

$$h_{1t} + (h_1\theta(x))_x = 0, \quad \text{with } \theta(x) = 1 - h_0^2(S + P'(x)) + h_0 G(x). \tag{18}$$

Given arbitrary initial conditions $h_1(x,0) = H_1(x)$, it is in fact possible to write down the general solution to (18). If we set $\theta(x) = 1/\phi'(x)$ then the solution is given by

$$h_1(x,t) = \frac{H_1(q)\phi'(x)}{\phi'(q)} \tag{19}$$

where the parameter q is (implicitly) defined by

$$\phi(q) = \phi(x) - t. \tag{20}$$

(The fact that (19) is indeed the solution of (18) may most easily be verified by observing that

$$h_{1t} + \left(\frac{h_1}{\phi'(x)}\right)_x = \left[\frac{\phi'(q)H_1'(q) - H_1(q)\phi''(q)}{(\phi'(q))^2}\right]\left[\phi'(x)\frac{\partial q}{\partial t} + \frac{\partial q}{\partial x}\right]$$

and, from (20) we have

$$\phi'(q)\frac{\partial q}{\partial t} = -1, \quad \phi'(q)\frac{\partial q}{\partial x} = \phi'(x),$$

whilst evidently $h_1(x,0) = H_1(x)$.)

The somewhat awkward nature of (19) rather limits its practical use: nevertheless we can gain some insight into the evolution of disturbances by considering some of the properties of (18). First, we note that in regions where the air knife does not operate or the blowing is negligible, h_0 takes one of the values h_- or h_+, and (18) becomes

$$h_{1t} + (1 - Sh_0^2)h_{1x} = 0.$$

Disturbances therefore propagate as simple waves. Note also that, according to Figure 2, we have

$$1 - Sh_-^2 < 0, \quad 1 - Sh_+^2 > 0. \tag{21}$$

Thus waves that are initially generated below the air knife travel back down to the coating reservoir, and waves that are generated above the air knife travel up with the substrate. It should also be noted that in this simple analysis the surface tension term in (12) has been ignored - evidently surface tension will, in reality, act to damp the waves that are predicted by (21).

Let us now consider regions where the air knife is active. Here (18) becomes

$$h_{1t} + [1 - h_0^2(S + P'(x)) + h_0G(x)]h_{1x} =$$

$$h_1[2h_0'h_0(S + P'(x)) + h_0^2P''(x) - (G(x)h_0)']. \tag{22}$$

We note that the term multiplying h_{1x} on the left hand side of (22) can only act to excite waves, while the term on the right hand side will determine whether or not the waves that are excited grow or decay. Clearly waves will grow if they are generated at a position where

$$2h_0'h_0(S + P'(x)) + h_0^2P''(x) - (G(x)h_0)' > 0. \tag{23}$$

Where is this condition most likely to be satisfied? First, we note that, where the blowing is maximum (at $x = x_m$, say), we expect to have $h_0(x_m) > 0$, $h_0'(x_m) < 0$, $P'(x_m) = 0$, $P''(x_m) < 0$, $G(x_m) = 0$ and $G'(x_m) > 0$. Every term in (23) is therefore either zero or negative at $x = x_m$, and there can be no question of instability. Note, however, that we expect that at some locations $x > x_m$ we will have $h_0'(x) > 0$, $G'(x) < 0$, and possibly $P''(x) > 0$ too. It is therefore likely that at some locations (23) will be satisfied. Indeed, it may easily be shown that, for the example (17) shown in Figure 3, for values of x greater than about 0.8, the condition (23) is satisfied.

It is also of interest to determine what will happen to the shape of such a disturbance. Since the speed of the disturbance is determined by its height, we can infer that in the downstream region there may be a region in which the value of $\frac{dx}{dt}$ is smaller if h is larger, so that a bump will break backward, while a depression will steepen at its front and broaden at

the rear end. This effect on an initial depression may ultimately lead to it breaking backward into itself, thus creating the bump seen at the front of the pock marks.

In order to test all of these possibilities, it was necessary to develop a numerical scheme. In what follows, such a scheme was used to test several scenarios. A full range of simulations could not be performed because of time constraints, but sufficient results were obtained to indicate that further investigation of these scenarios is worthwhile.

5 Numerical studies

It is of interest to examine a few cases in which a steady solution is disturbed in some way to see what will happen to the disturbance. In order to perform such tests, an accurate numerical scheme is required, and after some experimentation with Lax-Friedrichs and Lax-Wendroff techniques, it was decided that a characteristics approach would be more accurate. Equation (12), for the evolution of the surface height of the coating, can be arranged into the more convenient form,

$$h_t + \left(1 + hG(x) - h^2(S + P'(x))\right) h_x = \frac{1}{3}h^3 P''(x) - \frac{1}{2}h^2 G'(x). \tag{24}$$

In this equation, as previously, the surface tension term has been dropped. In the usual way, the characteristic traces can be written as

$$\frac{dt}{1} = \frac{dx}{1 + hG(x) - h^2(S + P'(x))} = \frac{dh}{\frac{1}{3}h^3 P''(x) - \frac{1}{2}h^2 G'(x)}$$

and since the equations are autonomous, we have two first-order ordinary differential equations for h and x, i.e.

$$\frac{dx}{dt} = 1 + hG(x) - h^2(S + P'(x)), \qquad x(0) = x_0 \tag{25}$$

$$\frac{dh}{dt} = \frac{1}{3}h^3 P''(x) - \frac{1}{2}h^2 G'(x), \qquad h(0) = h_0 \tag{26}$$

where x_0 and h_0 are values of x and h on the initial shape of the surface. These two differential equations can be solved using fourth-order Runge-Kutta integration along each characteristic starting at different values of x.

Starting with an initial condition of the steady solution for a particular case, then perturbing slightly by the introduction of a pock mark or bump, the evolution of the disturbance can be followed very accurately using a routine such as ODE45 in `Matlab` or *lsode* in Octave. The results of such simulations indicate that it is possible in certain circumstances for the disturbance to persist and steepen or potentially break.

5.1 Results

The first case shown is the perturbation to the steady state surface shape given by $\delta(x) = -0.08e^{-x^2}$, where the pressure and shear distributions for the steady-state solution are those used in Figure 3, i.e. $P(x) = 2e^{-x^2}$, $S = 0.5$ and $G(x) = 2x/(1 + x^4)$. Results are shown for a depression and a bump. The plot gives the evolved perturbation at time intervals 3 units apart. Note that all points on the surface to the left of the critical point move further to the left (i.e. drain back down into the bath), and so any disturbance in that region can not evolve

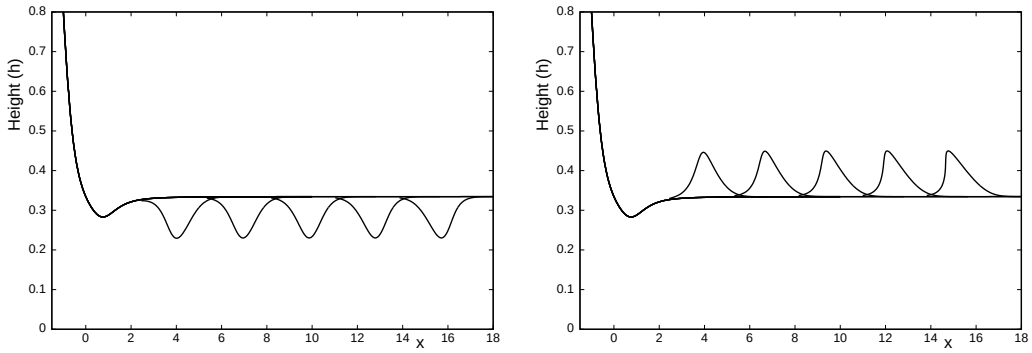

Figure 4: Fate of a depression and bump perturbation as time evolves. Each bump/depression is separated by $\Delta t = 3$ time units. Here, $P(x) = 2e^{-x^2}, S = 0.5$ and $G(x) = 2x/(1 + x^4)$. (The unperturbed solution, as in Figure 3, is also shown.)

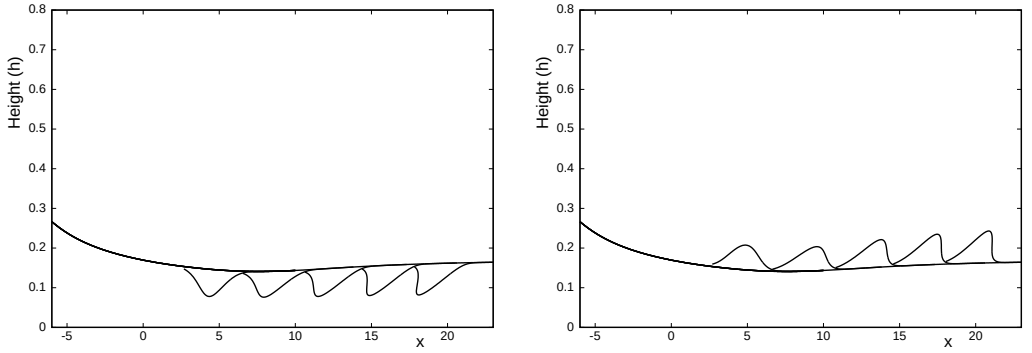

Figure 5: Fate of a depression and bump perturbation as time evolves. Each bump/depression is separated by $\Delta t = 3$ time units. Here, $P(x) = e^{-0.2x^2}, S = 0.5$ and $G(x) = 0.5x/(1+0.1x^4)$. (The unperturbed solution, as in Figure 3, is also shown.)

downstream. Bumps have a tendency, as predicted, to break downwards, while hollows have a tendency for the leading edge of the hole to steepen while the trailing end levels out. Figure 4 shows that neither disturbance appears to grow or decay, but it is clear that the trailing edge of the bump steepens more rapidly than the leading edge of the depression. Thus eventually the front of a pock mark will collapse back into the hole, perhaps explaining the bump at its leading edge. The fact that the disturbance appears to retain its amplitude is due to the narrowness of the air jet in this example. The conditions under which it will grow or decay no longer apply once it leaves the region of influence of the air knife.

To further observe these effects, Figure 5 shows the results for a case in which the region of influence has been greatly increased. In this example, $P(x) = e^{-0.1x^2}, S = 0.5$ and $G(x) = 0.5/(1 + 0.1x^4)$. It is clear that the steady-state solution is now much more spread, and that the bump perturbation grows and steepens at its leading edge while the depression grows slightly and steepens at its trailing edge. In this slightly artificial case the shear is much larger than the pressure effect.

Finally, we considered a case in which the pressure and shear are perturbed in time, and no spatial perturbation is made. Simulations here are slightly more difficult because we must

see the evolution of the whole coating. In the spatial perturbation case, we need only track the characteristics of the bump/depression as they move downstream, but here we must track the whole surface. Points originally located to the left of the critical point will move left (back toward the bath), while those downstream move further downstream. This leads to a rapid loss of resolution near to the central part of the flow region. To counteract this, a point re-distribution must be performed regularly during the simulation.

However, preliminary results indicate that the disturbance to the coating of a 10% Gaussian blip in the air pressure and shear induced by the jet causes only small variations to the shape of the coating. These travel in both directions along the surface of the coating, although those travelling to the left are irrelevant to the final shape. However, the shape of the coating does not return to the steady value as quickly as when perturbed spatially. The results of these simulations are quite hard to see and hence have not been included. Further simulations of this type would seem necessary.

These results indicate that various scenarios are possible depending on the pressure and shear induced by the jet. This is consistent with the findings of BlueScope Steel, and further work will involve detailed simulations using realistic pressure and shears such as those in Tu *et al.* [6] for the particular cases of interest.

6 Heat transfer

The effect of the large temperature variations in the system, and specifically their likelihood of contributing to the observed defects, is examined through a heat transfer model. In particular, we wish to determine whether there is a likelihood of a significant thickness of the coating beginning to solidify while it is within the influence of the air-knife and shortly downstream thereof.

It is reasonable to assume that upon leaving the alloy bath the steel strip is at the same temperature as the coating, as the timescale for the steel to heat to the bath temperature is approximately

$$\tau = \frac{\rho_s C_{p_s} d^2}{k_s} \sim 0.16, \tag{27}$$

where C_{p_s} is the specific heat, k_s is the thermal conductivity and d is the half-width of the steel strip. Therefore, most of the sheet will be at the bath temperature before the sheet exits. The only place that the heat can escape is from the outer surface, exposed to the air. The cooling of the much more massive steel sheet will dominate the cooling of the coating.

A significant proportion of the cooling from the surface will take place near the jet where the convective loss is highly forced. Here we provide a simple argument that parallels a more sophisticated analysis performed by Elsaadawy *et al.* [1]. These latter authors concluded that radiative losses only become relevant outside of the region of influence of the air jet and so we ignore them. Assuming steady, uni-directional flow and that diffusion along the sheet is much less than losses through the surface, the usual heat transport equation

$$\rho_s C_{p_s} \left(T_t + uT_x + wT_z\right) = k_s(T_{xx} + T_{zz}), \tag{28}$$

reduces to

$$\rho_s C_{p_s} uT_x = k_s T_{zz}, \tag{29}$$

where the boundary conditions are that there be no heat flux through the middle of the steel sheet (by symmetry), i.e.

$$T_z = 0 \quad \text{on} \quad z = -d \tag{30}$$

and heat loss to the air

$$k_s T_z = -\beta_a(x)(T - T_a) \quad \text{on} \quad z = h(x,t) \tag{31}$$

where we recall that $h(x,t)$ is the width of the molten coating, and $\beta_a(x)$ is the heat transfer coefficient to the air depending on the presence of the air jet. $T_a \approx 50°C$ is the air temperature near the strip. Elsaadawy *et al.* [1] obtained values for β_a ranging from $100 - 900$ W m^{-2} K^{-1} in the region of the jet. However the peak values are confined to a narrow region very close to $x = 0$.

Equation (29) can be integrated with respect to z to give

$$\rho_s C_{p_s} \int_{-d}^{h} u T_x dz = [k_s T_z]_{-d}^{h}\,. \tag{32}$$

Applying the boundary conditions, and treating the coating as part of the dominant steel sheet,

$$\rho_s C_{p_s}(h + d) U T_x = -\beta_a(x)(T - T_a). \tag{33}$$

Note that $h + d$ ($h << d$) is the thickness of the sheet plus coating, and U is the upward speed of the sheet. Averaging the heat transfer coefficient from Figure 13 in [1], $\beta_a(x) \approx 400$, and solving for $T(x)$ gives

$$T(x) \approx T_a + (T_B - T_a)\exp(-(x - x_B)/31) \tag{34}$$

where x_B is the height of the alloy bath and T_B its temperature. Now using $T_B = 460$, and a solidification temperature of $T_M = 420$, gives an estimate for the solidification point as $x_M - x_B \approx 3.6$m above the point at which the strip leaves the bath. This is an estimate of the distance travelled before most of the coating would become solid.

The more sophisticated analysis of Elsaadawy *et al.* [1] included radiation effects. Their estimate, which may be more accurate, has a worst case of $x_M \approx 0.44$m above the air jet for the point at which the surface begins to solidify. They obtained values of around 13m for 80% solidification. These values suggest that the solidification of the molten coating does not occur until some distance outside of the region where the layer thickness is set, and hence can be neglected for the purposes of most calculations in this work. However, it is clear that this is not a simple calculation and further work may be necessary to confirm this.

7 Mechanisms for creating surface indentations

In this section we consider mechanisms, specifically collision, for creating a local indentation in the surface of the coating fluid that might develop to become a pock-mark deformity.

Various mechanisms can be considered as possible sources of surface indentations. The MISG group debated the likelihood of these with advice from the industry representatives. Dissolved bubbles in the coating metal seem unlikely although further experiments might explore the possibility of entrainment of bubbles. There is an ongoing industrial investigation of the possibility of contamination. Vapour explosions, such as would occur if drops of

water were sprayed at the coating, were ruled out by the industry representatives. The most promising remaining possibility seemed to be the impacts of small particles (dust, oil, etc.) embedded in the air jets, which might fracture the oxide layer that forms on the surface of the coating. We shall consider this possibility in the following paragraphs.

It should be noted that from an initial indentation, further evolution of the fluid may be required to form the observed blemishes.

7.1 The Oxide film

An oxide film rapidly forms on exposed surfaces of the molten coating metal. In particular, the freshly exposed surface of molten metal above the jet-stripping line will soon begin to oxidise. The region of interest above the stripping line, within which the damage occurs, is slightly smaller than a centimetre high and the strip speed is about 2.5 m s^{-1} and so the oxide formation occurs on a timescale of 2-3 milliseconds. There is limited information available on the mechanical properties of the oxide layer, however, it will affect surface properties such as surface tension. There is no apparent effect on the macroscopic fluid flow.

7.2 Impacts of particles

We need to determine whether a particle embedded in the air jet will impact with the surface and if so at what velocity. The underlying velocity profile for the air jet and associated conditions are derived from experimentally measured results [6]. For these the jet nozzle is at 0.0256 m from the sheet with a nozzle velocity of 27.6 m s^{-1}. Based upon Figure 3 in [6], the air velocity profile along the central stagnation streamline can be set as approximately constant for the first 70% of the distance travelled towards the stagnation point, and thereafter it satisfies the Hiemenz solution form $u = -cx$.

In this expression, x is the horizontal perpendicular distance from the surface of the metal alloy coating and u is the fluid speed in this direction ($u = dx/dt$). The Hiemenz form will govern the fluid motion if we take the effective starting position x_0 to be 0.3×0.0256 m and the initial velocity for the fluid flow and particle to be $v_0 = -27.6$ m s^{-1}. Again referring to Figure 3 in [6], the value of c can now be set at $-v_0/x_0 = 3594$ s^{-1}.

Considering a small particle exiting the jet nozzle within the air flow along the central stagnation streamline, we can take the motion of this particle to satisfy

$$\tau \frac{dv}{dt} = u - v, \tag{35}$$

where v is the velocity of the particle, u is the velocity of the fluid, and

$$\tau = \frac{1}{18} \frac{d^2}{\mu} \rho_p \tag{36}$$

(cf. [2], equations (7.21) and (6.5)). In the expression for τ, ρ_p is the density of the particle which we shall assign to be 1000 kg m^{-3}, μ is the viscosity of the air which we take to be approximately 2×10^{-5} kg $m^{-1}s^{-1}$ (temperatures are modestly elevated near the sheet), and d is the diameter of the particle for which we consider values of order ten microns (1×10^{-5} m).

Combining $u = -cx$ and (35) we have a differential equation for the position of the particle x,

$$\tau \frac{d^2x}{dt^2} + \frac{dx}{dt} + cx = 0. \tag{37}$$

[Note that this equation could also be written in terms of just velocity v and position x as $\tau dv/dx + 1 + cx/v = 0$.] For values of c and τ close to the ones present here, the solution of equation (37) takes the form

$$x = e^{-\frac{t}{2\tau}} \left(x_0 \cos\left(\frac{\sqrt{4\tau c - 1}}{2\tau}\, t \right) + \frac{(2v_0\tau + x_0)}{\sqrt{4\tau c - 1}} \sin\left(\frac{\sqrt{4\tau c - 1}}{2\tau}\, t \right) \right). \tag{38}$$

The particle collides with the surface at a time

$$\frac{2\tau}{\sqrt{-1 + 4\,\tau\, c}} \arctan\left(\frac{x_0 \sqrt{-1 + 4\,\tau\, c}}{-2\, v_0\, \tau - x_0} \right). \tag{39}$$

At the wall the particle velocity can be simplified to

$$-\sqrt{\frac{v_0^2\tau + v_0 x_0 + x_0^2 c}{\tau}} \exp\left(\frac{\arctan\left(\frac{x_0\sqrt{-1+4\,\tau\, c}}{2v_0\tau + x_0} \right)}{\sqrt{-1 + 4\tau c}} \right). \tag{40}$$

If we substitute in the values of v_0, x_0 and c assigned above and take $d = 1 \times 10^{-5}$ m, so that $\tau = 1/3600$ s, then the particle will collide with the wall after about 3.4 milliseconds (from the position x_0) with a velocity of about 15 m s^{-1}.

7.3 Impacts - energy analysis

To estimate whether a particle can break the oxide layer we compare the work required to create a hole with the kinetic energy of the particle. The corresponding energy balance equation is

$$W\, A = \frac{1}{2} m v^2, \tag{41}$$

where W is the work that must be done per unit area to break the oxide layer, A is the area of destruction of the oxide layer (the size of the hole), and m and v are the mass and velocity of the particle.

Using experimental information on oxide formation and strength for aluminium (at temperatures of 700 °C and above) [3] we may estimate an approximate value for W. Extrapolating [3], Figure 2, we estimate 1 nm for the thickness of the oxide layer at the height where the air knives are encountered. (In comparison the overall metal film coating thickness is around 5-10 μm.) For this thickness ([3], Figure 9), W is approximately 0.5 N m^{-1}.

We now suppose that the impacting particle is of order 10 μm diameter with density 1000 kg m^{-3}. Then to create a hole the size of the particle ($A = 10^{-10}$ m^2) would require a velocity of about 10 m s^{-1}. This is lower than the velocity for such a particle on the central stagnation streamline calculated above (15 m s^{-1}), and so it seems likely that such a particle could fracture the oxide layer.

To create a hole by this mechanism of the size of the observed pockmarks ($A = 10^{-6}$ m^2) the energy required would be much higher and would require a particle of the order of a thousand times more massive with $d \sim 100$ μm.

8 Conclusions

This proved to be a very rich problem. The equations derived for the development of the molten coating approximate very closely the steady-state behaviour experienced in practice. In fact, variants on the original work of Thornton, Tu and Tuck [4, 5, 7] are used to perform in-line calculations. The success of this model gives every confidence that the unsteady equations can accurately predict the behaviour of the system across the full range of parameters in use today. Therefore this work should be able to reproduce the effects seen in the factory if the correct form of the pressure and shear due to the air knife are incorporated.

It seems likely that during the coating process there are disturbances created. In normal operating conditions these previously dissipated to nothing, but with the changes to new coatings these are now persisting long enough to become a problem. A detailed investigation of the parameter space using the numerical method should reveal under what circumstances this occurs.

In addition to the spontaneous disturbances due to the air knife, vibration etc., the group has considered the possibility of impact creating small craters, and was unable to dismiss them as a possible cause. Again, the discussion above is relevant, since no matter how a disturbance forms, it is unimportant if it decays. The solidification of the molten metal has been shown to occur beyond the region of interest and so the pivotal matter to the group seemed to be the stability problem.

Future work will be used to confirm and refine some of the preliminary results. It would be desirable to find surface trajectories for more realistic pressure/shear terms. Using the full partial differential equation could show how an initial distortion will evolve: it could be used to consider whether small ripples could cause the line/wave defects that have also been observed.

A Typical parameter values

The list below gives typical values used in this work.

- C_p = specific heat of zinc alloy coating ≈ 388 J kg^{-1}K^{-1}
- C_{p_s} = specific heat of steel ≈ 700 J kg^{-1}K^{-1}
- d = half-width of the steel strip $\approx 10^{-3}$m
- g = gravitational acceleration ≈ 9.8 m s^{-2}
- γ_0 = surface tension coefficient of the coating layer $\approx 10^{-1}$ N m^{-1}
- h_0 = length scale of the thickness of the coating layer $\approx 10^{-5}$ m
- k_a = thermal conductivity of air ≈ 0.026 Wm^{-1}K^{-1}
- k_s = thermal conductivity of steel ≈ 30 Wm^{-1}K^{-1}
- k = thermal conductivity of zinc alloy coating ≈ 100 Wm^{-1}K^{-1}
- L = length scale in upwards direction - half-width of air jet $\approx 5 \times 10^{-3}$m
- μ = dynamic viscosity of the coating $\approx 10^{-3}$ kg m^{-1}s^{-1}

- ρ = density of the coating $\approx 3 \times 10^3$ kg m^{-3}, ρ_s = density of steel $\approx 7 \times 10^3$ kg m^{-3}
- U = upward speed of the metal sheet ≈ 2.5 m s^{-1}
- U_a = maximum centerline speed of the air jet ≈ 28 m s^{-1}
- T_M = melting point of zinc alloy coating ≈ 420 °C
- T_B = typical bath temperatures ≈ 460 °C

Using these values, the scalings for the pressure and shear stress and the non-dimensional quantities that appear are

- Pressure scaling $\frac{\mu U}{\epsilon^2 L} \approx 10^5$ kg m^{-1}s^{-2}, Shear scaling $\frac{\mu U}{\epsilon L} \approx 600$ kg m^{-1}s^{-2}
- Capillary number (Surface tension) Ca= $\frac{\mu U}{\gamma_0} \approx 2 \times 10^{-2}$
- Reynolds number Re = $\frac{UL}{\mu} \approx 12$
- Stokes number $S = \frac{\rho g h_0^2}{\mu U} \approx 0.001$, Length ratio $\epsilon \approx 2 \times 10^{-3}$

Acknowledgements

We are grateful to the industry representatives Cat Tu and Daniel Yuen for their support and enthusiasm. We also thank the other people who participated in this project who included Chris Breward, Phil Broadbridge, Andrew Dixon, Nev Fowkes, Tony Gibb, Robert McKibbin and Astri Sjoberg.

References

[1] Elsaadawy, E.A., Hanumanth, G.S., Balthazaar, A.K.S., McDermid, J.R., Hrymak, A.N. & Forbes, J.F. (2007) Coating weight model for the continuous hot-dip galvanizing process, *Metallurgical & Materials Trans. B*, **38B**, 413-424.

[2] Reist, P.C. (1993) *Aerosol Science and Technology (2nd edition)*, McGraw-Hill, New York.

[3] Syvertsen, M. (2006) Oxide skin strength in molten aluminium, *Metallurgical & Materials Trans. B*, **37B**, 495-504.

[4] Thornton, J.A. & Graff, H.F. (1976) An analytical description of the jet-finishing process for hot-dip metallic coatings on strip, *Metallurgical & Materials Trans. B*, **7B**, 607-618.

[5] Tu, C.V. (1990) Optimisation of lip gap for thin film coating in the jet stripping process, *Proc. 5th Int. Conf. Manufacturing Engineering*, University of Wollongong, Australia.

[6] Tu, C.V., Wood, D.H. & Hooper, J.D. (1994) Small distance impingement of a plane jet, International Colloquium on Jets, Wakes and Shear Layers, Melbourne, Australia, 18-20 April 1994.

[7] Tuck, E.O. (1983) Continuous coating with gravity and jet stripping, *Phys. Fluids*, **26** (9), 2352-2358.